Applied Catalysis B: Environmental 319 (2022) 121889

Contents lists available at ScienceDirect

Applied Catalysis B: Environmental

journal homepage: www.elsevier.com/locate/apcatb

Catalytic aldol condensation of bio-derived furanic aldehydes and acetone: Challenges and opportunities

Alberto Tampieri [a,b], Karin Föttinger [b,*], Noelia Barrabés [b], Francesc Medina [a,*]

[a] Chemical Engineering Department (DEQ), ETSEQ, Universitat Rovira i Virgili, Avinguda dels Països Catalans 26, 43007 Tarragona, Spain
[b] Institute of Materials Chemistry, Technische Universität Wien, Getreidemarkt 9/BC, 1060 Wien, Austria

ARTICLE INFO

Keywords:
Aldol condensation
Hydrotalcite
In situ/operando
ATR-IR
NMR

ABSTRACT

Bio-derived furfural and 5-hydroxymethylfurfural can be combined with acetone to yield aldol condensation products that may serve as biofuel and polymer precursors. We have explored different catalytic systems to obtain and purify each product in the most efficient way. The results of the catalytic tests of the cross-condensations and of the self-condensation of acetone allowed the comparison of the different reactivity of the two aldehydes. Online and *in situ/operando* ATR-IR was used to monitor the reaction over time and to study the interaction of the reaction species with the solid catalyst, especially the formation of deactivating organic matter that covers the surface, which is a major issue in heterogeneous condensation processes. *In situ* NMR was used to study the ongoing reaction, assessing its stereoselectivity, and to study the behavior of deuterated species in the catalytic system. Finally, the preparation of C14, a hetero-double-condensation product, was also explored.

1. Introduction

Fossil resources are running out, prompting industries and the scientific community to develop alternative transportation technologies based on renewable resources [1]. Drop-in biofuels might fill the gaps where dense energy sources are required (e.g. aviation fuels) [2]; however, current renewable hydrocarbon-producing technologies, such as the Fischer-Tropsch synthesis, are unable to achieve a narrow distribution of chain lengths [3], and deoxygenative processing of biomass yields carbon numbers typically below the gasoline/diesel range [4]. The group of Dumesic reported in 2004 the conversion of carbohydrates to alkanes, whose molecular weights are again too low to serve as transportation fuels [5]. The same group then developed a strategy based on aldol condensations to combine furfural and 5-hydroxymethyl furfural (HMF), dehydration products of xylose and glucose [6], respectively, with acetone, which can also be obtained from biomass [6], yielding desirable and targeted chain lengths [7]. Total hydrodeoxygenation (HDO) of the condensates leads to the corresponding linear alkanes [8]. The low stability of HMF and the elusiveness of a cost-effective method for its synthesis hinders the large scale production of this aldehyde [9], which is considered a "sleeping giant" of sustainable chemistry [10]. Its high price is probably the main reason why HMF is underrepresented in the field of catalytic aldol condensations compared to furfural.

The formation of the double-condensation product of HMF with acetone (also known as C15) is catalysed by aqueous NaOH [11], which is convenient because C15 precipitates in water due to its low solubility, allowing its selective isolation in good purity [11]. The same applies to the product of the double-condensation of furfural with acetone (C13); the catalytic medium may be reused multiple times after filtration with negligible loss of activity and selectivity [12]. These advantages outweigh the reactor corrosion and expensive wastewater treatments associated with the use of caustics [13], and this is the reason why the aqueous processes have the highest potential for industrial applications. Mineral acids can also be used as catalysts, although they are often avoided as they trigger the formation of byproducts such as levulinic acid and humins [9,14]. The selective preparation and purification of the mono-condensation products C8 and C9 is more difficult. The excess acetone required to attenuate the double-condensation promotes its self-condensation, yielding byproducts diacetone alcohol (DAA) and mesityl oxide (MES). The use of heterogeneous catalysts would facilitate the separation from the products, and they could be designed to minimize byproduct formations and selectively obtain the mono-condensation products [15,16]. Over the years, several heterogeneous catalysis-based processes for the aldol condensation of HMF and furfural with acetone have been reported [15,17–20], including

* Corresponding authors.
E-mail addresses: karin.foettinger@tuwien.ac.at (K. Föttinger), francesc.medina@urv.cat (F. Medina).

https://doi.org/10.1016/j.apcatb.2022.121889
Received 7 June 2022; Received in revised form 11 August 2022; Accepted 22 August 2022
Available online 24 August 2022

systems working under neat conditions [16,21–24]: in this case, the higher solubility of the condensates in acetone may prevent the deactivation due to surface deposition [17]. C13 and C15 can be used as organic dyes due to their optical properties [11], and their total HDO products may serve as jet fuels [25]. C13, C15 and their partial HDO derivatives can also serve as monomers and cross-linking agents [26], and the same could be said for C8 and C9 [27,28].

In the present work, we have studied the aldol condensation of furfural and HMF with acetone using catalysts with different properties and under different conditions, exploring the challenges and opportunities of the research field. We have addressed aspects often overlooked in other reports such as the purity and stability of the reaction components and their behaviour and interaction with the catalyst, the reaction stereochemistry, and the concurrent acetone self-condensation. Moreover, we studied the preparation of a C14 molecule, the hetero-double condensation product of furfural, HMF and acetone. Finally, we used an array of spectroscopic techniques to gain insights into the catalytic processes: *ex situ* FT-IR and UV-Vis in the solid state to characterize the deactivating organic matter that deposits on the catalyst; *ex situ* UV-Vis in the liquid phase to study the evolution of the spectra with the reaction; online and *in situ/operando* ATR-IR to monitor the reaction and adsorption of species, and the formation of the organic deposit; and *in situ* NMR to study the formation of elusive transient species.

2. Experimental section

We synthesized and purified, by column chromatography (Section A2), the reaction species to have spectroscopic references, to use them in adsorption studies and as quantification standards in catalytic tests. The double-condensation products were prepared in aqueous NaOH-catalysed, exploiting the favourable precipitation of the condensates, whereas the mono-condensation products were purified from the crudes of the cross-aldol condensation catalytic tests in acetone, where the second condensation is unfavourable. The aldol intermediate C8-OH was synthesized in the aqueous phase using L-lysine as a catalyst. The starting material furfural was distilled under vacuum, while HMF was recrystallized in Et_2O. The NMR spectra of the pure compounds were recorded on a Bruker Avance Neo 400 (400 MHz), or a Bruker Avance 400 (400 MHz) at room temperature. ^{1}H NMR spectra in $CDCl_3$ are reported in parts per million (ppm) downfield of TMS and were measured relative to the signals for $CHCl_3$ (7.26 ppm). All ^{13}C NMR spectra were reported in ppm relative to residual $CHCl_3$ (77.2 ppm) and were obtained with ^{1}H decoupling. The coupling constants, *J*, are reported in hertz (Hz).

The solids used as heterogeneous catalysts were all derived from the same 2:1 Mg:Al hydrotalcite (HT), prepared by coprecipitation of Mg and Al nitrates in presence of NaOH and Na_2CO_3; HT is a layered double hydroxide (LDH) that contains water and carbonates in the inter-layer. On calcination, the LDH structure collapses and converts HT into a mixed metal oxide (MMO). The meixnerite-like solid (MX) was obtained by liquid-phase rehydration of MMO, which restores the LDH structure and introduces water and hydroxyls in the inter-layer. The details of the preparations are reported elsewhere [22]. The catalytic tests of the cross-aldol condensations of acetone with the furanic aldehydes were performed neat in a 250 mL round bottom flask (rbf) with 100 mL of acetone, 2 g of aldehyde and 0.4 g of catalyst (1:5 catalyst:aldehyde w-w). The solution was brought at reflux (56 °C) under magnetic stirring and then the solid catalyst was added (time zero event). 1 mL of mixture was taken at the corresponding time, and the internal standard was added (20 μL of toluene). Then, the mixture was filtered through a membrane filter (Chromafil Xtra PTFE-20/25, pore size 20 μm, Macherey-Nagel) and analysed by GC-FID (GC-2014 with AOC-20i, Shimadzu, equipped with an HP-5 column (30 m x 0.32 mm x 0.25 μm film thickness)). After reaction the mixture was let cool down and filtered off through quantitative filter paper (DP 1506 110, Hahnemühle). The solid ("recovered catalyst") was washed with 50 mL of pure acetone, and it was left drying under air at room temperature for 1 day. The procedure for the dehydration of C8-OH was adapted from this one: 1.604 g of C8-OH were dissolved in 50 mL of acetone in a 100 mL rbf, and 0.2 g of catalyst.

The *ex situ* FT-IR characterizations were performed in ATR mode, using a Spectrum 400 spectrometer, Perkin Elmer, equipped with a GladiATR accessory, Pike (128 scans at a 4 cm^{-1} resolution between 400 and 4000 cm^{-1} (MIR), and between 600 and 40 cm^{-1} (FIR)), or a FT/IR 6700 Jasco spectrometer, with a TGS detector and equipped with an ATR PRO ONE accessory (32 scans at a 4 cm^{-1} resolution between 400 and 4000 cm^{-1}). The solids were analysed in the form of powder, whereas the liquids were analysed by putting a drop on the crystal to cover it.

The *ex situ* UV-Vis characterizations were performed in samples contained in cuvettes (QS high precision cell made of quartz Suprasil, light path 10 mm, Hellma Analytics). The analyses in the solid state were performed with Lambda 750 UV-Vis spectrometer, PerkinElmer, in diffuse reflectance in the 200–2000 nm range at room temperature and ambient atmosphere; $BaSO_4$ was used to perform blanks, and to dilute solid and liquid samples. The analyses in the liquid phase were performed with a UV-1600PC spectrophotometer, VWR or with a V-630 spectrophotometer, Jasco (recorded in absorption from 200 to 1000 nm, 1.0 nm interval); the spectrum of the solvent, either acetone or water, is used as a background. For the study of an NaOH-catalysed reaction, a 5 mL reaction mixture of 5:1 ACE:FUR (acetone:furfural) in water ([FUR] = 0.2 M) was prepared. NaOH (10 mol%) was added to start the reaction, which was run at room temperature under magnetic stirring. The mixture was sampled (50 μL) before the addition of NaOH and 2 h after that, and then diluted with deionized water in a 100 mL volumetric flask.

ATR-IR online and *in situ/operando* analyses (Section B4.1) were performed with a Vertex 70 (Bruker Optics) spectrometer equipped with a liquid nitrogen-cooled mercury cadmium telluride (MCT) detector and a commercial mirror unit (SN 854) (Figure B80). The cell (composed of a metallic structure that held the trapezoidal ZnSe ATR internal reflection element (45°, 52(48) mm x 20 mm × 2 mm, Crystran) and the EPDM rubber gasket (70° Shore A, Semperit E9566, Persicaner & co GmbH)) was placed on the beam path in a vertical position inside a Plexiglas box under reduced pressure. The solution was pumped in and out with a peristaltic pump (ISM831C, Ismatec) at 0.1 mL/min through rubbery tubes for peristaltic pumps (Ismatec, Tygon 2001), using PTFE tubes for the rest of the tubing. The spectra are taken at a rate of one every 5 min, from 800 to 4000 cm^{-1}, 25 scans per analysis (100 for the background), at a 4 cm^{-1} resolution.

All NMR analyses using No-D acetone as the solvent (pure compounds and DOSY) involve a glass capillary containing D_2O for the lock. The spectra were reported in ppm relative to ACE (2.05 ppm). The same applies to the estimation of the C13:C14:C15 ratio in ACE-FUR-HMF experiments, for which the sample is prepared by dissolving the filtered reaction crude in ACE, followed by transferring the solution to an NMR tube and inserting the D_2O capillary. The C13:C14:C15 ratio is then estimated from the spectra as described in Section C1.5 A. In the *in situ* analyses, the spectra were reported in ppm relative to the 6 H signal of DAA (1.16 ppm) as the one of ACE was decoupled to increase the signal-to-noise ratio. The *in situ* reaction was catalysed by MMO (50 mg for ACE-FUR, 70 for ACE-HMF); after introducing the solid, a mixture of 10 mg of aldehyde in 0.5 mL of acetone was introduced slowly to avoid catalyst; finally, the D_2O capillary was introduced, and the sample was analysed. After shimming, the acetone signal was decoupled and the spectrum was recorded; the tube was recovered and sonicated at room temperature. Then, the analysis was repeated. In the *in situ* analysis of ACE-d_6-FUR and ACE-d_6-HMF reactions, ACE-d_6 was used for the lock directly; the reaction was scaled up from 0.5 mL to 0.7 mL, using proportional amounts of reagents and catalyst. The reaction crudes were also analysed by GC-MS (gas chromatograph 6890 Series equipped with an automatic liquid sampler (HP7683 Series) and mass spectrometer

(5973 Hewlett Packard), the column used was a HP-5MS (30 m x 0.25 mm x 0.25 μm) from Hewlett Packard). The sample was prepared by filtering first through a cotton plug and then a filter (PTFE-HI, 13 mm, 0.2 μm, Agilent Technologies). No-D acetone was used to perform a 1 to 10 dilution.

3. Results and discussion

3.1. Catalytic tests

2:1 Mg:Al hydrotalcite and related basic materials were used as catalysts because our own and related works showed their outstanding performance in aldol condensation [21–23,29]; solid bases seem to be more suitable for this process as compared to acids like zeolites (Section B1), as they are more active at low temperatures [30]. Moreover, simple procedures can be used to change the basic properties of the solids from weak Brønsted basicity of the HT, to strong Lewis basicity of the MMO, to strong Brønsted basicity of the MX [31]. Water is produced in the condensation, which could interact the catalyst, possibly affecting the mechanism and alter its structure (e.g. rehydration); it should also be noted that HT and MX contain water in the interlayer, and this might also play a role in the process.

The activity trend observed in the ACE-FUR reaction (MX > MMO >> HT) is typical for this type of catalytic system (Fig. 1.a-c) [32]. The influence of sodium, which originates from the HT synthesis and is known to increase the activity of these catalysts [33], can be excluded since the Na content of this batch, as determined by ICP, is 90.45 μg/g, much below the accepted threshold of 0.04%. C8-OH and C8 are initially present in comparable amounts; the situation changes over time as the former progressively depletes by dehydrating to the latter. The large excess of acetone favours the mono-condensation, even though the formation of C13 is not completely suppressed. When we used pure C8-OH to study the activity of the catalysts as "dehydrators", MMO proved to be the fastest (Fig. 1.d), seemingly contradicting the ACE-FUR results. However, this is only a symptom of the complex behaviour of heterogeneous catalysts in aldol condensations: the solids generally change colour over time as they accumulate species on the surface and deactivate [32], and the colouration of the recovered catalysts after the C8-OH dehydration is darker than the same after ACE-FUR (Figure B4); it appears to be the case that the high concentration of C8-OH enhances the rate of deactivation and that MMO would be the catalyst that best copes with the higher concentration of aldols in the mixture.

Although ACE-HMF is generally regarded as slower than ACE-FUR [17], proper comparisons of the two reactions under the same conditions are rare in the literature; in our case, HMF does undergo a substantially slower reaction (Fig. 1.e-g). Besides, the activity pattern of the three catalysts (MX >> HT > MMO) is off [22]. As for the selectivity, C9-OH is not detected while, once again, the excess acetone does not prevent the formation of the double condensation product C15. Furfural is known to undergo degradation under normal storage conditions [34], and for this it is commonly distilled as a means of purification. The group of Kubička has recently reported the impact of the time of furfural

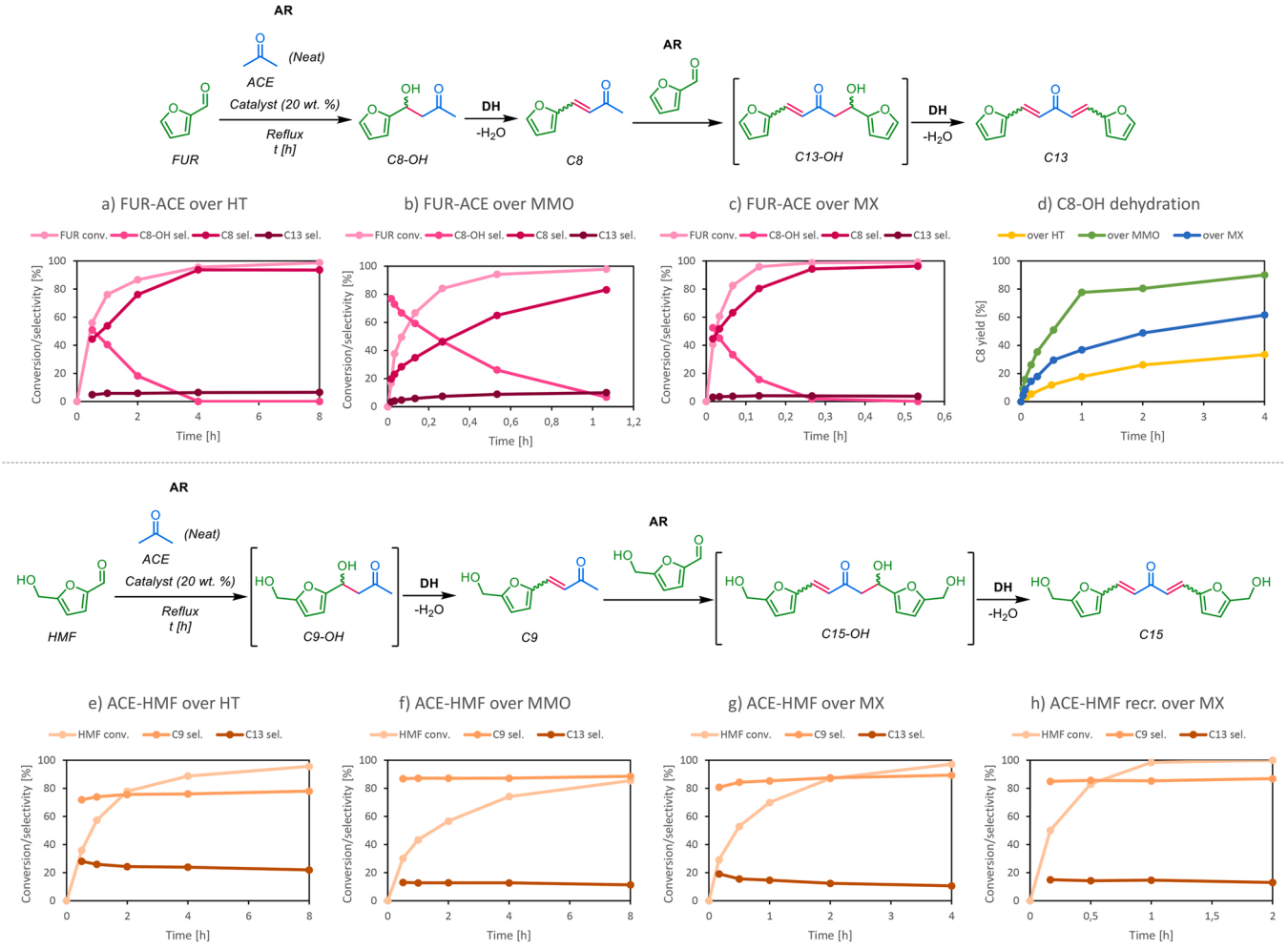

Fig. 1. Results of the cross-aldol condensation of acetone with furfural (a-c), with HMF (e-h), and C8-OH dehydration (d); reaction conditions: 2 g of aldehyde and 0.4 g of catalyst in 100 mL acetone, reflux at atmospheric pressure. AR: Aldol Reaction; DH: DeHydration.

storage on a very similar system to ours [35]. We hypothesized that the HMF purity may have an effect on the catalytic activity, as it does for furfural. Possible impurities/degradation products are cirsiumaldehyde (Scheme B1), the product of the self-etherification of HMF [36]; levulinic acid, which forms together with formic acid; and humins [14]. We sought to get rid of the impurities of HMF by recrystallization in Et_2O [36], which allowed us to separate a black tar from our starting material (Figure A2). The MX-catalysed condensation using the recrystallized HMF proved to be noticeably faster than before, albeit still slower than its corresponding ACE-FUR reaction (Fig. 1.h). Our results point to a process that is regulated by the adsorption of species on the surface. HMF and derivatives can establish multiple H-bonds with solids, and indeed they are much more strongly retained in chromatography (Figure A5). These molecules may also undergo hydroxyl deprotonation, which would establish an electrostatic interaction: if our catalyst can deprotonate acetone ($pKa \sim 20$), required for the "activation" of acetone (enolization) [37], then the alcohols ($pKa \sim 15$) should readily deprotonate too [38]. These phenomena may explain why with HMF the reaction is slower (slower desorption and turnover), the activity pattern is off (complex interaction with the catalyst), and the aldol intermediate is not seen (C9-OH sticks to the surface until dehydration). In addition, the strong adsorption of C8/C9 may also promote the second condensation event, providing an explanation for why the double condensation is more frequent than it should.

During the catalytic tests, the concurrent self-ketol condensation of acetone (ACE-ACE) was studied. The formation of DAA in the ACE-FUR catalytic tests follows the typical trend of catalyst activities (Fig. 2.a-c). The same is true for the ACE-HMF test, which corroborates the oddity of HMF behaviour in the condensation. However, in all cases the self-ketol reaction of acetone to DAA is faster in presence of FUR than with HMF, and when no aldehyde is in the mixture the self-ketol is much faster. This points towards an inhibiting effect of the aldehydes and/or their derivatives on the DAA formation, possibly because of the presence of strongly adsorbed species that modulate the self-condensation. Both the aldol and the ketol reactions share the acetone enolization pathway [37]; however, the ketol reactions are slower than aldols because aldehydes are more electrophilic than ketones [38]. Hence, the presence of aldehydes should increase the average rate of C-C bond forming steps; this is clearly not the case (Table 1). The use of recrystallized HMF does not appear to affect the DAA formation. MMO and MX are very fast in producing DAA, whose concentration reaches a plateau in a matter of minutes in the absence of aldehydes. This plateau concentration, about 0.35 M DAA (~ 5 wt%), is apparently the equilibrium concentration of DAA in acetone under our reaction conditions. Indeed, the equilibrium of the ketol formation is generally shifted towards the reactants [39], and at reflux this concentration should be around 5 % (Figure B1). To prove this, we prepared a solution of about 0.8 M DAA in acetone and introduced MMO under the same conditions. As expected, the concentration of DAA sharply decreases (Fig. 2.d); what's more, the formation of MES does not really follow a specular profile to the one of DAA consumptions, implying that the ACE/DAA equilibrium is very fast. Importantly, no detectable DAA and MES formation were experienced in an ACE-ACE blank reaction.

Table 1
Initial rates expressed in $mmol_{SPECIE} \cdot g_{CAT}^{-1} \cdot h^{-1}$; reaction conditions as in the experiments in Fig. 1 and 2; in Table B1 are the same values normalized for the catalyst surface area, concentration of basic sites, and equivalent mass.

Event	HT	MMO	MX
FUR conv.	58.2	524.5	1267.0
HMF conv.	28.5	23.9	69.4
HMF_{recr} conv.	/	/	119.3
DAA_{FUR} prod.	10.3	364.3	932.8
DAA_{HMF} prod.	0.8	16.0	24.4
$DAA_{HMFrecr}$ prod.	/	/	22.5
DAA_{ACE} prod.	68.4	2940.2	7783.0
DAA cons.	/	7610.1	/

3.2. IR and UV-Vis characterisations

We previously characterised the catalysts by PXRD, ICP-AES, ESEM-EDX, TEM, FT-IR, Raman, N_2 physisorption, CO_2-TPD and TGA-MS [22], finding that the structure and morphology of the solids are not overly disrupted after the process and that deactivating organic matter was deposited on the surface. FT-IR spectroscopy proved to be the most valuable tool to study this organic deposit, and in this work it was used to characterise the recovered catalysts. In the spectra of the LDHs, the 1650–1500 cm^{-1} range is occupied by the signal of an H_2O bend [40]; the spectra of HT_{rec}^{FUR} and MX_{rec}^{FUR} (Fig. 3.a), which are HT and MX recovered after ACE-FUR reactions, respectively, possess an overlapping peak at ~1580 cm^{-1}. This is the region of C=C bonds, and the peak pattern does not match with the ones of the molecular species. As for the C8-OH dehydration, the two recovered LDH catalysts HT_{rec}^{C8OH} and MX_{rec}^{C8OH} both present similar peaks that may be a component of the broad peak of the catalysts recovered after ACE-FUR. In neither MMO_{rec}^{FUR} nor MMO_{rec}^{C8OH} any such signal is detected. Conversely, the recovered

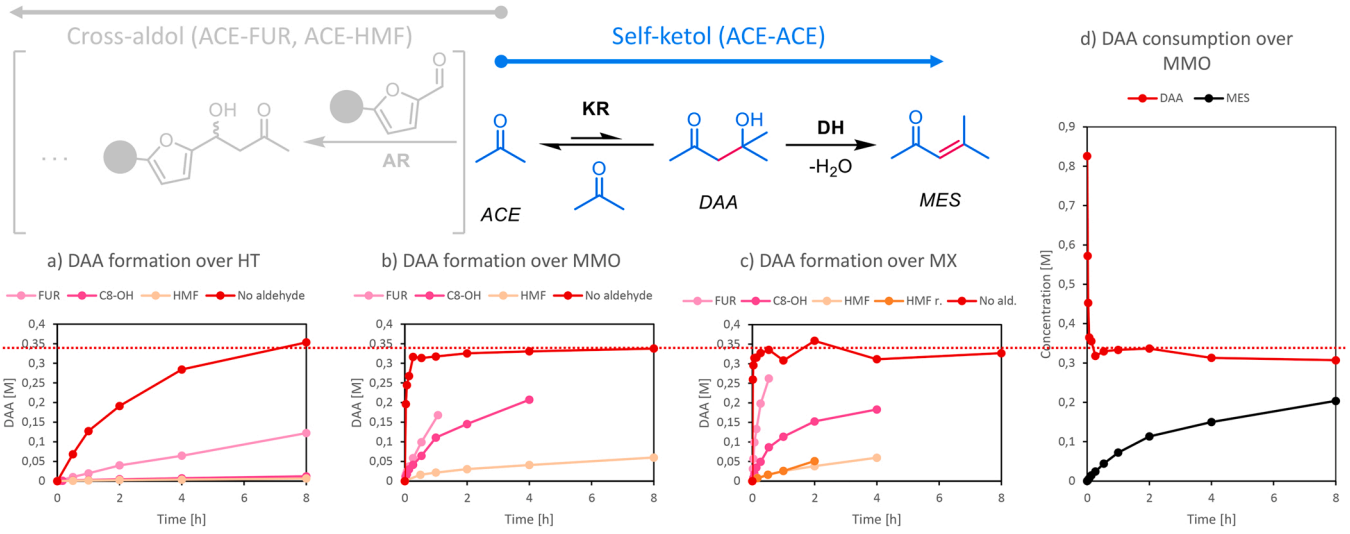

Fig. 2. Results of the self-ketol reaction of acetone; reaction conditions: 2 g (or 0 g) of aldehyde (or 0.8 M DAA) and 0.4 g of catalyst in 100 mL acetone, reflux at atmospheric pressure. KR: Ketol Reaction.

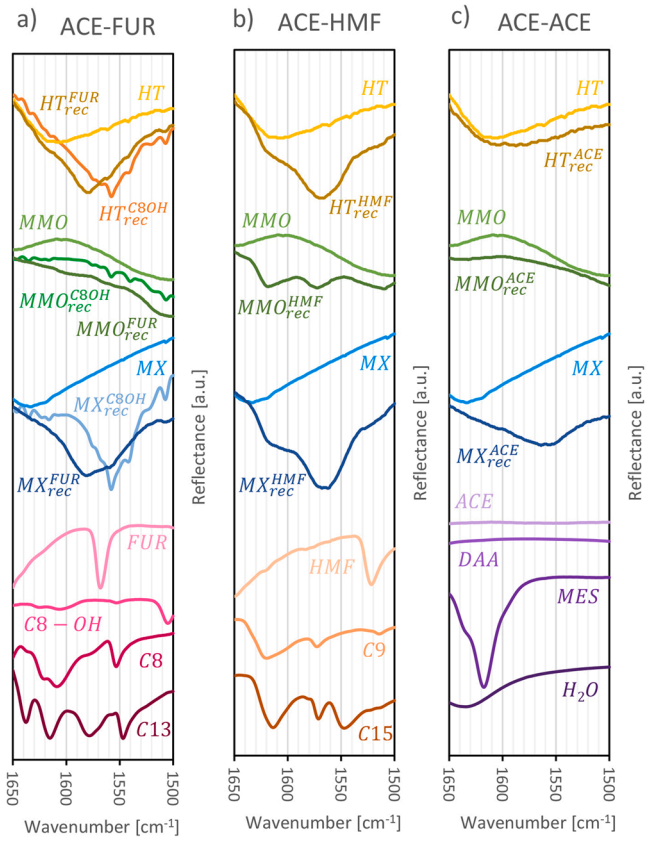

Fig. 3. FT-IR characterization of the pure reaction species and fresh and recovered catalysts of a) ACE-FUR reactions; b) ACE-HMF reactions; c) ACE-ACE reactions.

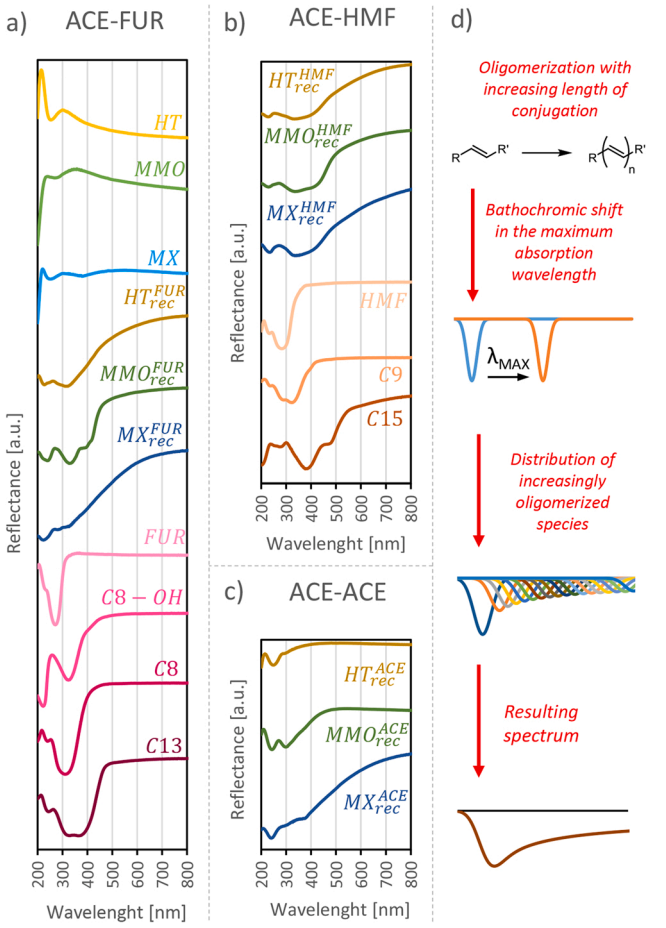

Fig. 4. UV-Vis characterization of the pure reaction species and fresh and recovered catalysts of a) ACE-FUR reactions; b) ACE-HMF reactions; c) ACE-ACE reactions; d) effect of the conjugation on the UV-Vis spectrum of molecules.

HT_{rec}^{HMF} and MX_{rec}^{HMF} both present a peak in a similar position (at ~1570 cm^{-1}, Fig. 3.b). This time, MMO_{rec}^{HMF} does present some peaks in this region and they appear to belong to C9, the major reaction product, which was perhaps retained in an adsorbed form. Finally, in the spectra of the recovered LDHs after ACE-ACE, while a broad peak is formed at 1560 cm^{-1} for MX_{rec}^{ACE} (Fig. 3.c), no change is seen for HT_{rec}^{ACE}, which is likely due to the low activity of HT; MMO_{rec}^{ACE} exhibits no signal.

Since the colouration of the catalysts after the reaction is evident (Figure B4), we resorted to UV-Vis diffuse reflectance spectroscopy to characterise the deposited organic matter. The spectrum of the white, fresh catalysts is rather featureless (Fig. 4.a). On the other hand, HT_{rec}^{FUR}, MMO_{rec}^{FUR} and MX_{rec}^{FUR} all exhibit broad peaks in this range; however, while the intensity of the peak of MMO_{rec}^{FUR} appears to decrease relatively abruptly, the peaks of both HT_{rec}^{FUR} and MX_{rec}^{FUR} show a decay that extends well into the visible range at high wavelengths. In the case of MMO_{rec}^{FUR} the colour appears to originate from deposited molecular species involved in the reaction such as C8 and C13; for the recovered LDHs, it appears like highly conjugated species are present, as conjugation leads to a bathochromic shift in the maximum absorption wavelength (Fig. 4. d). The same discussion applies to the HMF-related recovered catalysts (Fig. 4.b). While HT_{rec}^{ACE} and MMO_{rec}^{ACE} exhibit faint signals, perhaps related to adsorbed small molecules (Fig. 4.c), MX_{rec}^{ACE} takes on a brownish colour with related tailing, a symptom of the presence of conjugated acetone byproducts. As the colour change of the catalyst is a potential source of important information about what happens on its surface, we studied the liquid phase component by UV-Vis spectroscopy to assess the feasibility of *in situ/operando* experiments [41]. Acetone as a solvent covers the low wavelength range and suppresses all signals, although the higher wavelengths involved in the deactivation should be accessible (Section B3.1). In water, the peaks of ACE and DAA partially overlap with the one of HMF (Fig. 5.a), whereas the signals of C9 and C15 are redshifted as a result of conjugation. The same effect is experienced with FUR, C8 and C13 (Fig. 5.b), while for C8-OH the maximum absorption wavelength is very low due to the disruption of the conjugation. A catalytic experiment was performed to test the applicability of the technique in real conditions, namely in a NaOH-catalysed ACE-FUR (Fig. 5.c). After the reaction, the peak of FUR is replaced by the ones of the products, and it can be seen how the reaction conditions favoured C8 over C13.

3.3. Online and in situ/operando ATR-IR studies

ATR-IR spectroscopy proved in the past to be useful for the characterization of heterogeneous catalysts in *operando* conditions [41,42]. We used this technique to obtain more information about the formation and identity of the organic deposit. Our system consisted of a flow cell comprising a ZnSe ATR crystal, which was employed with and without a catalyst thin film deposited on the surface (Fig. 6.a). We first dissolved our pure compounds in acetone to build a library of spectra (Section B4.2), and then performed online reactions with MX (Fig. 6.b). In this mode, a background is taken when acetone is flown in the cell; the cell is then connected to a vessel containing the reaction solution and recirculated; finally, when the signal is stable, MX is introduced in the outer vessel and the analysis starts. The spectrum changes over time as the ACE-FUR reaction takes place (Fig. 6.c). The formation of DAA is apparent but, luckily, the ACE-ACE does not affect the C═C and C═O

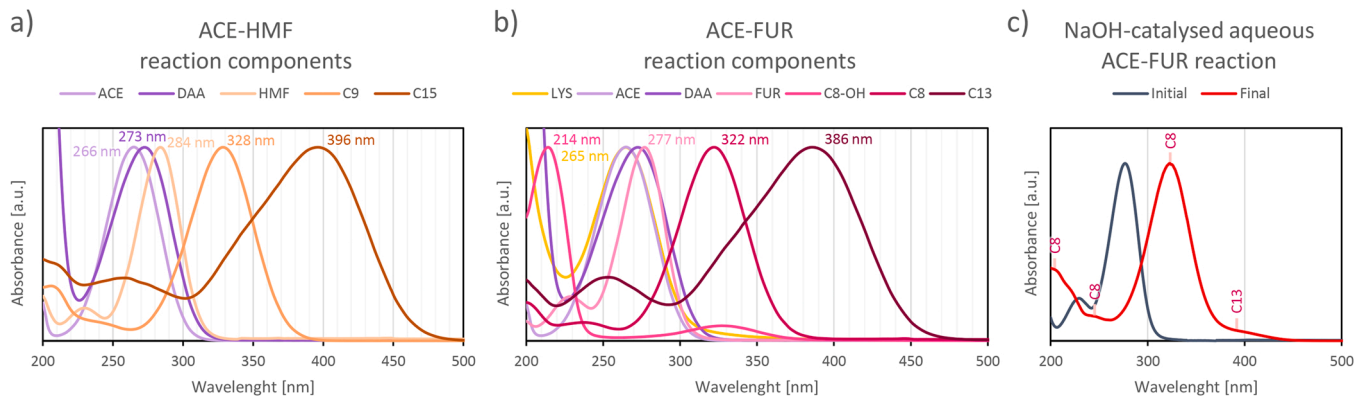

Fig. 5. UV-Vis spectra in water: a) ACE-HMF reaction components; b) ACE-FUR reaction components; c) samples prepared from an initial and final reaction solution of an NaOH-catalysed aqueous ACE-FUR.

area, although the signal of water, peaking at 1645 cm^{-1}, does. The C═C region is dominated by the rising C8 olefinic peak. C8-OH is detected by the presence of a signal at 1505 cm^{-1}, while the concentration of C13 is very low. In ACE-HMF, the formation of C9 seems to be slower and the DAA formation is suppressed, in line with the catalytic results (Fig. 6.d); the signals of C15 are hidden by the overlaying peaks.

We then tested the catalytic system in *in situ/operando* conditions (Fig. 6.b). In the first part of this experiment, MX is deposited on the ATR crystal, the cell is assembled and acetone is flown through it. When the signal is stable, the background is recorded and the acetone feed is changed for the reaction solution. In the ACE-FUR spectra obtained at these conditions vast areas of signal suppression are present (Fig. 6.e), due to the MX spectrum in the background. Moreover, a set of negative DAA peaks appeared: the spectrum of the DAA formed in the pretreatment is included in the background; its concentration then decreases during ACE-FUR as the initial DAA is flushed out while the formation of new DAA is hampered by the reaction. These issues do not involve the C═C and C═O spectral range, which experiences a broad intensity increase in the same area as the signal of the organic deposit detected by conventional FT-IR characterization. In the ACE-HMF *operando* spectra (Fig. 6.f) a similar broad peak of the organic deposit is formed during the reaction, and the intensity of the negative DAA peaks is higher, which reflects the higher ACE-ACE suppression under these conditions. Our setup allows us to change the medium and wash the catalyst with acetone after reaction (Fig. 6.b). This allows to observe the relative order in which the various species are desorbed from the catalyst: for instance, when washing after the ACE-FUR reaction (Fig. 6.g), a sharp C8 C═O peak appears where there was before just a shoulder in furfural's one, whereas after ACE-HMF (Fig. 6.h) the differential disappearance of HMF and C9 is even clearer, pointing to stronger adsorption of condensates over aldehydes. Moreover, the signal of the deposited matter can be isolated after cleaning, revealing a broad bump peaking at 1580–1590 cm^{-1} for ACE-FUR and an intense broad peak centred at about 1570 cm^{-1} for ACE-HMF. In the C═O area no residual peak is seen; other peaks at lower wavenumbers, perhaps hidden by the spectrum of the LDH in the conventional *ex situ* FT-IR characterization, appear after washing. HT behaves much like MX in both ACE-FUR and ACE-HMF, giving rise to analogous broad peaks (Figures B114 and B136). MMO, on the other hand, appears to catalyse the ACE-FUR reaction without leaving any residue (Figure B120). Interestingly, the two peaks visible in the recovered MMO_{rec}^{HMF} also appear in the MMO-catalysed ACE-HMF spectrum after washing (Figure B142).

Finally, we performed adsorption experiments of the reaction intermediates and products to study their interaction with the catalyst (Fig. 7). C8-OH and C8 leave broad peaks both of which are very similar to each other and to the one of the ACE-HMF. In turn, the ACE-HMF peak is almost identical to the one of C9, implying that the deactivation in ACE-HMF proceeds via oligomerization of C9, while in ACE-FUR multiple pathways happen, among which is one pathway through C8 that is equivalent to the one of ACE-HMF. C13 has an adsorption residual peak that, combined with the one of C8, seems to match pretty well the overall ACE-FUR peak; C15 does not seem to contribute much to the one of ACE-HMF. Interestingly, C8 does not leave any trace in an adsorption study on MMO (Figure B160).

In light of the results presented so far, it appears like the absorption band in the C═C range originates from ketol oligomerizations, which we propose as the main deactivation pathway (Scheme 1). In shortage of aldehydes, the C8/C9 enolate may "actively" attack other ketones such as acetone (to form oligomer #2) or another C8/C9 (oligomer #3), which may be trapped on the surface by virtue of their stronger adsorption/insolubility. In parallel, C8/C9 may lay "passively" on the surface and be attacked by acetone (oligomer #1), a scenario that is more plausible at conditions in which acetone's enolization (and DAA formation) is intense. We suppose that both pathways happen in different changing proportions according to the distribution of species. In this view, the active-type C9 oligomerization would be prominent in ACE-HMF, giving rise to the band centred at 1570 cm^{-1}, whereas in ACE-FUR both active- and passive-type oligomerizations occur, producing the broad bump around 1580 cm^{-1}. In C8-OH dehydration and C8-OH/C8 adsorption studies the concentration of product is the maximum from the very beginning and the active-type oligomerization will dominate, decreasing the activity and giving rise to a band similar to the one of ACE-HMF. C13/C15, like oligomers #2 and #3, cannot enolize but may be engaged in passive-type oligomerizations. We have previously detected oligomer #1 or #2 [22], and in a recent report ketol oligomerization species of ACE-FUR were detected, corroborating our hypothesis [43]. Other concomitant deactivation pathways may happen via Cannizzaro reaction of furfural [44], or of HMF [45], although we detected no corresponding alcohols in our mixtures (Section B1.3); or via Michael additions of the enones (Scheme B2) [46], although this oligomerization would break the conjugation and bring about a hypsochromic shift in the UV-Vis range instead of the tailings deep into the visible range observed. It is important to prevent a deactivation via formation of oligomers to avoid oxidative regenerations that may deteriorate the solid in the long run [22,47]. In this sense, MMO is particularly promising since, apparently, its organic deposit is just strongly adsorbed reaction species that could perhaps be cleansed.

3.4. *In situ* ^1H NMR studies

NMR spectroscopy distinguishes *E/Z* isomers by their coupling constants [48]. Our reaction should be *E*-selective [38], but it has been observed in the past that the reaction may initially produce *Z* isomers and only later the *E-Z* ratio is tipped over [19], which could have implications on the reaction mechanism. We performed an *in situ* reaction-in-a-tube NMR experiment to monitor the formation of

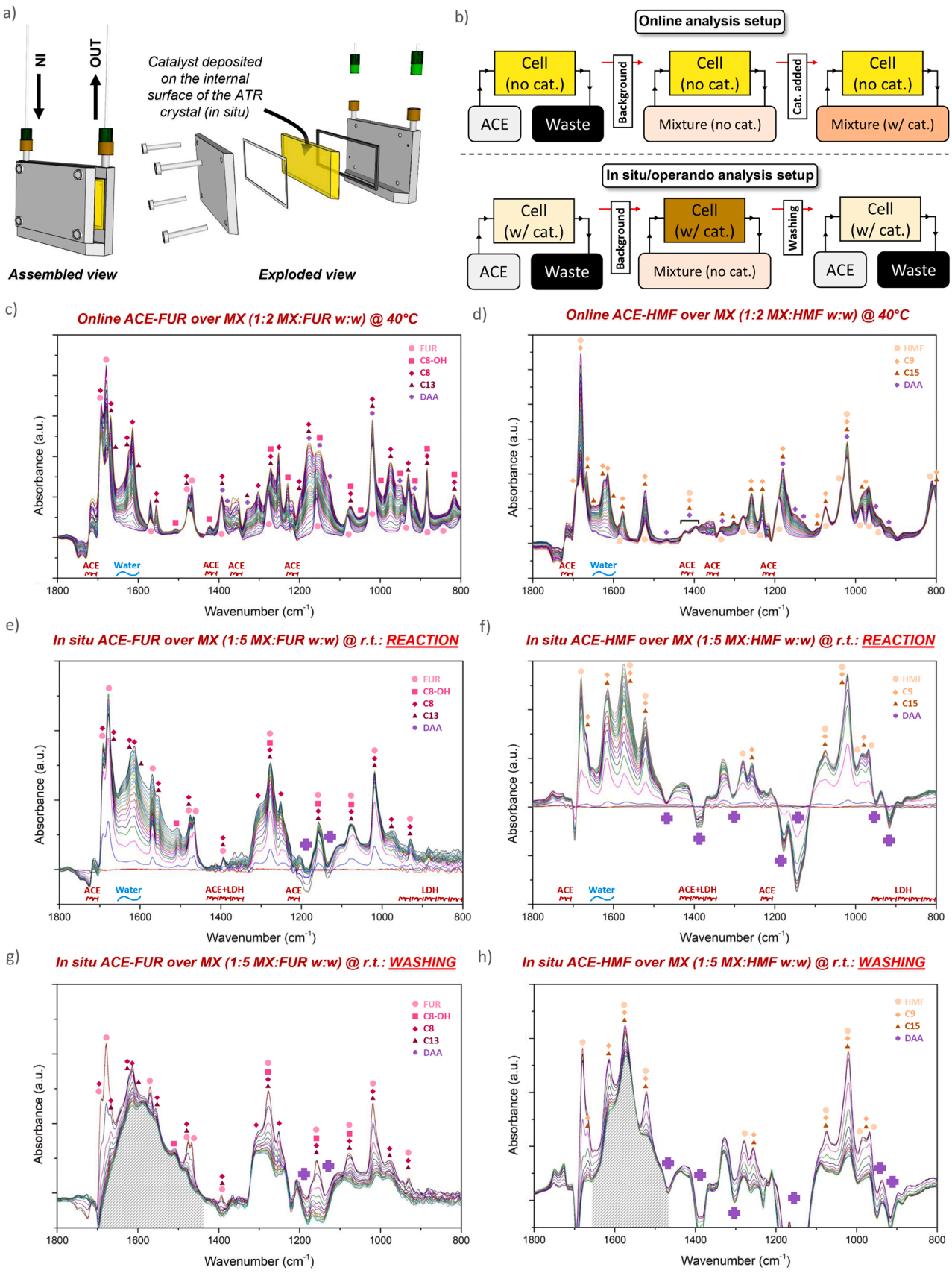

Fig. 6. ATR-IR analyses: a) scheme of the flow cell; b) diagrams of the analysis setups: in online processes the reaction is carried out in a separate vessel, flowing the solution in the cell to monitor the liquid phase in real time, whereas in in situ processes the reaction happens within the cell, and both the solid and the liquid phase are monitored simultaneously; results of the analyses over MX: c) online ACE-FUR; d) online ACE-HMF; e) in situ/operando ACE-FUR (reaction phase); f) in situ/operando ACE-HMF (reaction phase); f) in situ/operando ACE-FUR (washing phase); g) in situ/operando ACE-HMF (washing phase).

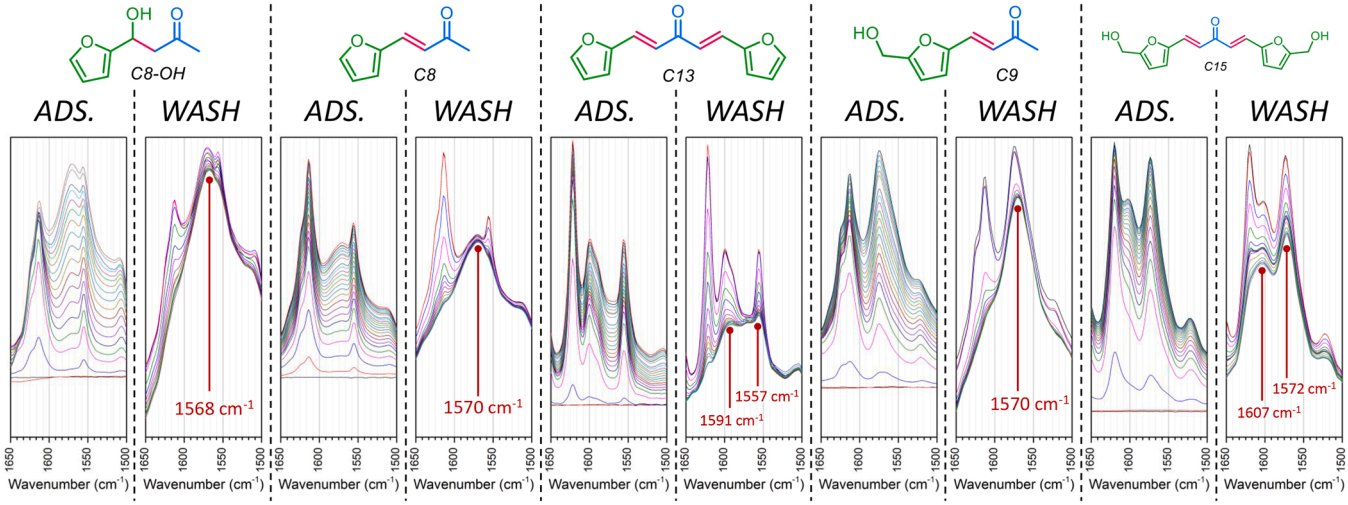

Fig. 7. Results of the ATR-IR in situ/operando adsorption studies.

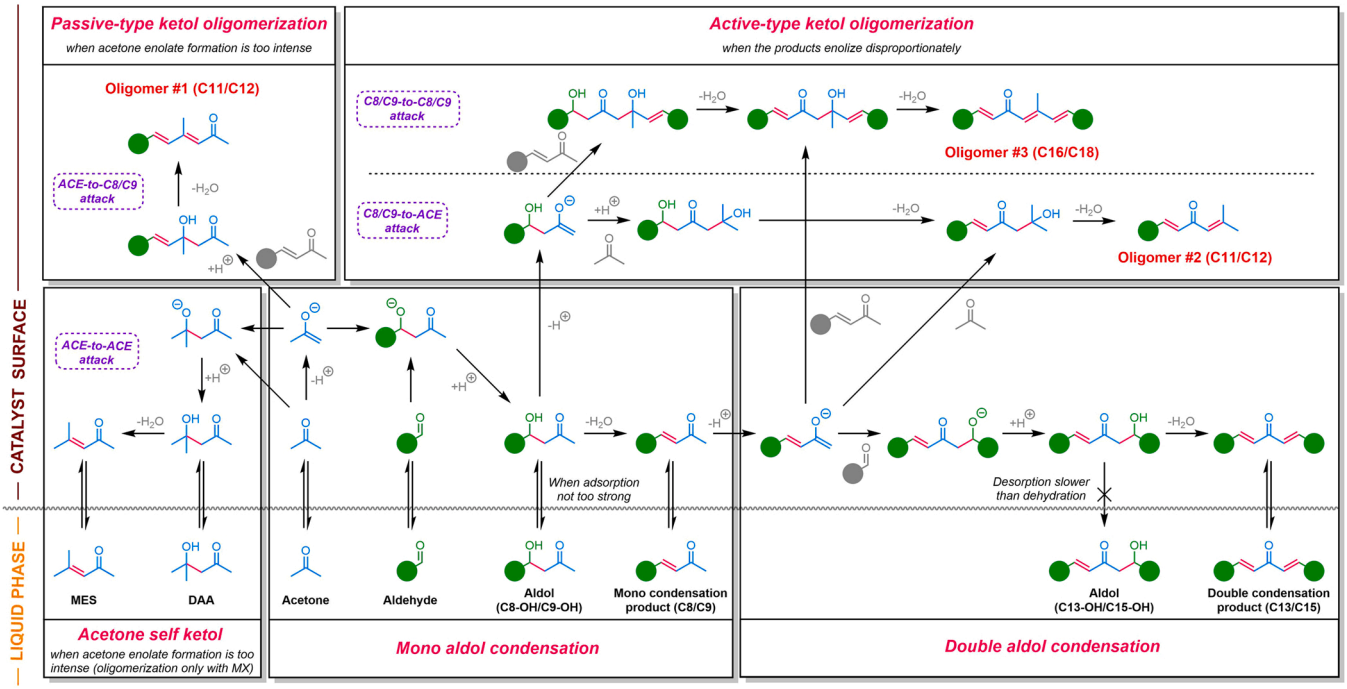

Scheme 1. Proposed reaction and deactivation mechanism.

transient species and the stereoselectivity of the reaction (Fig. 8.a). In the *in situ* ACE-FUR analysis, the most information-dense area of the spectrum is that of the aromatic and olefinic protons (Fig. 8.b), in which it is possible to see how furfural leaves place to the condensation products, while C8-OH appears and disappears over time. Importantly, only the *E*-isomer signals are visible, recognizable from the value of the coupling constants (J = 16.2–15.7 Hz), while among the low-intensity peaks none appears to possess the J of a *Z*-isomer (supposedly around 10.9 Hz [19]) (Figure C21). The ACE-HMF reaction over MMO is slower than the corresponding ACE-FUR, and for this a higher catalyst load was used (Fig. 8.c), again resulting in the exclusive formation of *E*-isomers of the condensation products. NMR spectroscopy can also be used to obtain the mass diffusivity D of the reaction components via DOSY (Section C1.2): D decreases with the molecular weight of the molecule, and HMF and derivatives diffuse slower than their FUR correspondents. While the process in the stirring flask of our catalytic tests should not be diffusion-limited, it is possible that the diffusion plays a role in the *in situ/operando* analysis (e.g. by limiting the condensation and or promoting the oligomerization) and, more in general, in continuous processes.

From our catalytic and spectroscopic results, it appears that dehydration is the rate-limiting step: the C-C bond forming step in ACE-ACE is evidently faster than the dehydration, the accumulation of C8-OH suggests that the same is true for ACE-FUR and, perhaps, ACE-HMF too. The elusiveness of C9-OH may originate from an even slower desorption step caused by the strong adsorption of HMF and its derivatives, which could also account for the slower reaction of HMF, with the dehydration limiting the turnover. The signal of C8-OH's benzylic proton is the only one appearing in the spectral range of 4.5–6.0 ppm (Fig. 8.d); C9-OH should possess a peak at a similar position that can be unequivocally assigned to it, and we could not clearly distinguish any signal from the baseline, corroborating its absence. Performing analogous *in situ* NMR

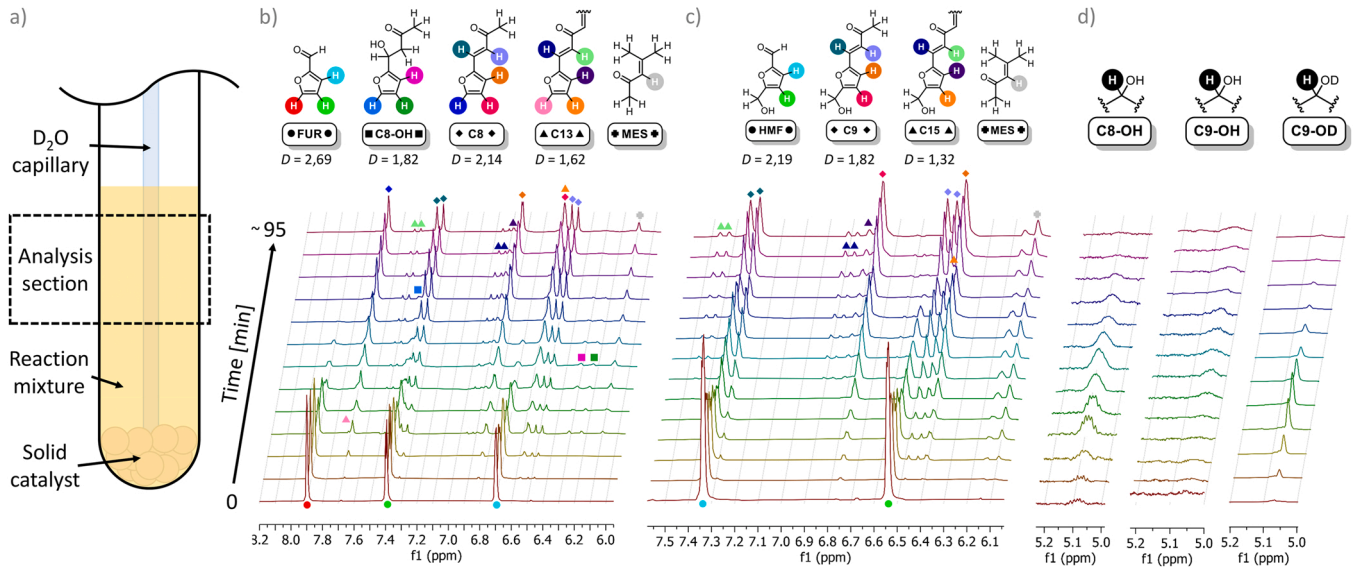

Fig. 8. In situ ^{1}H NMR studies: a) analysis setup; b) ACE-FUR spectra; c) ACE-HMF spectra; d) -C*H*OH- region.

experiments using deuterated acetone, we unveiled a kinetic isotope effect (KIE): C8-OH-d_6 (C8-OD) appears to be more persistent than C8-OH, likely because of the slower dehydration with α-deuterium atoms [49]; the KIE is even more apparent in the ACE-d_6-HMF reaction, where a specie identified as C9-OD is now a major component at early stages. It appears like the dehydration of C9-OD is so slow that it becomes slower than its desorption, allowing its accumulation in the liquid phase.

3.5. C14 and hetero-double condensations

After studying the aldol condensations of the two aldehydes separately, we wondered what would have been the result of a cross-condensation in the presence of both. We envisaged that such a reaction would lead to the formation of a hetero-double-condensation product, C14, which possesses a furyl group at one end and a hydroxymethyl furyl at the other. By performing a multicomponent aldol condensation in aqueous NaOH with a FUR:ACE:HMF molar ratio of 1:1:1, a product distribution close to 0.25:0.5:0.25 C13:C14:C15 is obtained (Scheme 2). Interestingly, this is the ratio that would be obtained with a purely statistical combination of aldehydes and ketones in the mixture. We also tested a 0.4:1:1.6 FUR:ACE:HMF ratio, and the product ratio we obtained almost perfectly matches the statistical distribution of 0.04:0.32:0.64 C13:C14:C15. These results do not highlight a difference in reactivity of the two aldehydes in a homogenous reaction, as opposed to their behaviour with solid catalysts. Our attempts to selectively synthesized C14 with a one-pot synthesis did not prove successful: the formation of C9 in situ comes with the double condensation to C15, leaving some acetone unreacted and affording some C13, in addition to C14, when FUR was added five minutes later. Finally, using use pure C9 and reacting it with the complementary FUR, we obtained C14 with complete selectivity; in this regard, the retro-aldol followed by homo-double-condensations to C13 and C15 proved not to be a problem.

The multicomponent synthesis may be used industrially to obtain a mixture of alkanes with tuneable properties from mixtures FUR and HMF (Figure C55): direct processing of biomass would afford both aldehydes (even in a controlled laboratory environment the dehydration of glucose yields mixtures of FUR and HMF [50]), and this could be a strategy to valorise them without the need of separation. Moreover, C14 may be prepared together with C15 by adding desired quantities of FUR and act as a chain-length regulator in C15 polymerizations [26]. HDO of C14 would allow to access tetradecane from biomass.

4. Conclusions

In conclusion, we used three spectroscopic techniques, ATR-IR NMR, and UV-Vis, to characterize reaction species and obtain information from the aldol condensation of acetone, furfural and HMF, outlining the differences between the reactions; in addition to providing mechanistic information, the three techniques may also be used for quantification in the liquid phase. Our results suggest that the adsorption has a crucial influence on the reaction outcome and catalyst deactivation, and that dehydration is a critical step as it appears to be rate-limiting in our process. Deuteration and hetero-condensations offer some possibilities for more in-depth mechanistic studies and may prove essential for the study of processes such as enolization and retro-aldols that are difficult to explore in other ways. We hope with our study to aid rational catalyst design and reaction optimization of our and other condensation systems. Future work should be directed towards the development of strategies to

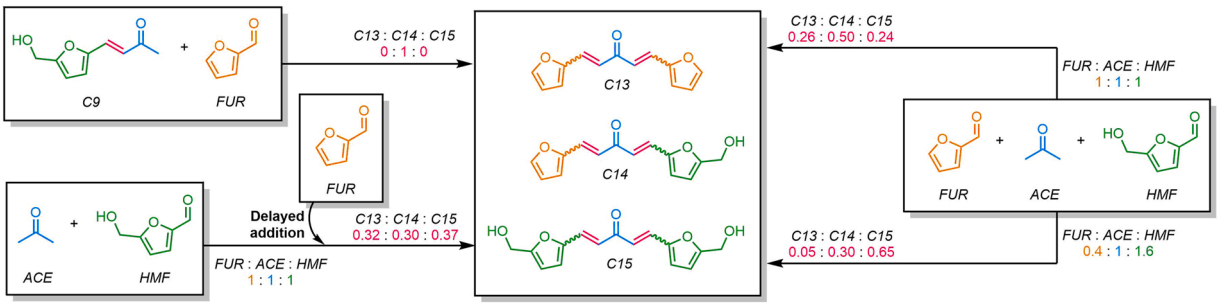

Scheme 2. Cross-condensation of FUR, ACE and HMF into C13, C14 and C15.

suppress the byproduct formation and catalyst deactivation by holding back the ketol reactions in favour of the aldols.

Supplementary materials

Supplementary materials available: in SM A are the details of the synthesis and purification of the pure starting materials, intermediates and products, and their characterization by ^{1}H- and ^{13}C NMR in $CDCl_3$; in SM B are the details of the catalytic tests, and of the spectroscopic experiments by FT-IR, UV-Vis, and online+*in situ/operando* ATR-IR; in SM C are the ^{1}H NMR studies performed in acetone and d^{6}-acetone (DOSY experiments, *in situ* studies with and without deuteration+GC-MS analysis of the crudes, and determination of the C13:C14:C15 ratio).

CRediT authorship contribution statement

A.T.: Conceptualization, Investigation, Writing – original draft. **K.F.:** Supervision, Writing – review & editing. **N.B.:** Supervision, Writing – review & editing. **F.M.:** Supervision, Writing – review & editing.

Declaration of Competing Interest

The authors declare that they have no known competing financial interests or personal relationships that could have appeared to influence the work reported in this paper.

Data Availability

Data will be made available on request.

Acknowledgements

A.T. thanks AGAUR, Spain (Generalitat de Catalunya) and ESF (European Social Fund) for his postgraduate scholarship (2018 FI_B 01124), and Fundació Universitat Rovira i Virgili for a project grant (B-2021/21). A.T. also thanks the European Union for an Erasmus Placement scholarship. This research was funded in part by the Austrian Science Fund (FWF) [SFB TACO, Grant number F81]. N.B. acknowledges support by the Austrian Science Fund (FWF) via grant Elise Richter (V831-N). F.M. thanks the Ministerio de Economía y Competitividad, Spain for financial support (RTI2018-098310-B-I00), as well as Proyectos de Generación de Conocimiento AEI/MCIN, Spain (PID2021-123665OB-I00). M. Weiss is acknowledged for the ICP measurements, C. Hametner and R. Guerrero for the NMR measurements, D. Cano for FT-IR measurements, and S. Abelló for the GC-MS measurements. M. Latschka, G. Pacholik, V. Truttman and F. Valentini are also gratefully acknowledged for the support they provided.

Conflicts of interests

The authors declare that they have no competing interests.

Appendix A. Supporting information

Supplementary data associated with this article can be found in the online version at doi:10.1016/j.apcatb.2022.121889.

References

[1] A. Ajanovic, R. Haas, Prospects and impediments for hydrogen and fuel cell vehicles in the transport sector, Int. J. Hydrog. Energy 46 (2021) 10049–10058, https://doi.org/10.1016/j.ijhydene.2020.03.122.
[2] W.-C. Wang, L. Tao, Bio-jet fuel conversion technologies, Renew. Sustain. Energy Rev. 53 (2016) 801–822, https://doi.org/10.1016/j.rser.2015.09.016.
[3] H. Gruber, P. Groß, R. Rauch, A. Reichhold, R. Zweiler, C. Aichernig, S. Müller, N. Ataimisch, H. Hofbauer, Fischer-Tropsch products from biomass-derived syngas and renewable hydrogen, Biomass Convers. Biorefin. 48 (2019) 22, https://doi.org/10.1007/s13399-019-00459-5.
[4] H. Li, A. Riisager, S. Saravanamurugan, A. Pandey, R.S. Sangwan, S. Yang, R. Luque, Carbon-increasing catalytic strategies for upgrading biomass into energy-intensive fuels and chemicals, ACS Catal. 8 (2018) 148–187, https://doi.org/10.1021/acscatal.7b02577.
[5] G.W. Huber, R.D. Cortright, J.A. Dumesic, Renewable alkanes by aqueous-phase reforming of biomass-derived oxygenates, Angew. Chem. Int. Ed. Engl. 43 (2004) 1549–1551, https://doi.org/10.1002/anie.200353050.
[6] L. Wu, T. Moteki, A.A. Gokhale, D.W. Flaherty, F.D. Toste, Production of fuels and chemicals from biomass: condensation reactions and beyond, Chem 1 (2016) 32–58, https://doi.org/10.1016/j.chempr.2016.05.002.
[7] G.W. Huber, J.N. Chheda, C.J. Barrett, J.A. Dumesic, Production of liquid alkanes by aqueous-phase processing of biomass-derived carbohydrates, Science 308 (2005) 1446–1450, https://doi.org/10.1126/science.1111166.
[8] Y. Nakagawa, S. Liu, M. Tamura, K. Tomishige, Catalytic total hydrodeoxygenation of biomass-derived polyfunctionalized substrates to alkanes, ChemSusChem 8 (2015) 1114–1132, https://doi.org/10.1002/cssc.201403330.
[9] H. Chang, I. Bajaj, A.H. Motagamwala, A. Somasundaram, G.W. Huber, C. T. Maravelias, J.A. Dumesic, Sustainable production of 5-hydroxymethyl furfural from glucose for process integration with high fructose corn syrup infrastructure, Green. Chem. 23 (2021) 3277–3288, https://doi.org/10.1039/d1gc00311a.
[10] K.I. Galkin, V.P. Ananikov, When will 5-hydroxymethylfurfural, the "sleeping giant" of sustainable chemistry, awaken? ChemSusChem 12 (2019) 2976–2982, https://doi.org/10.1002/cssc.201900592.
[11] H. Chang, A.H. Motagamwala, G.W. Huber, J.A. Dumesic, Synthesis of biomass-derived feedstocks for the polymers and fuels industries from 5-(hydroxymethyl) furfural (HMF) and acetone, Green Chem. 21 (2019) 5532–5540, https://doi.org/10.1039/c9gc01859j.
[12] M. Gu, Q. Xia, X. Liu, Y. Guo, Y. Wang, Synthesis of renewable lubricant alkanes from biomass-derived platform chemicals, ChemSusChem 10 (2017) 4102–4108, https://doi.org/10.1002/cssc.201701200.
[13] G.J. Kelly, F. King, M. Kett, Waste elimination in condensation reactions of industrial importance, Green. Chem. 4 (2002) 392–399, https://doi.org/10.1039/b201982p.
[14] S.K.R. Patil, C.R.F. Lund, Formation and growth of humins via aldol addition and condensation during acid-catalyzed conversion of 5-hydroxymethylfurfural, Energy Fuels 25 (2011) 4745–4755, https://doi.org/10.1021/ef2010157.
[15] W. Shen, G.A. Tompsett, K.D. Hammond, R. Xing, F. Dogan, C.P. Grey, W. C. Conner, S.M. Auerbach, G.W. Huber, Liquid phase aldol condensation reactions with MgO–ZrO2 and shape-selective nitrogen-substituted NaY, Appl. Catal. A: Gen. 392 (2011) 57–68, https://doi.org/10.1016/j.apcata.2010.10.023.
[16] T. Yutthalekha, D. Suttipat, S. Salakhum, A. Thivasasith, S. Nokbin, J. Limtrakul, C. Wattanakit, Aldol condensation of biomass-derived platform molecules over amine-grafted hierarchical FAU-type zeolite nanosheets (Zeolean) featuring basic sites, Chem. Commun. 53 (2017) 12185–12188, https://doi.org/10.1039/c7cc06375j.
[17] J. Cueto, L. Faba, E. Díaz, S. Ordóñez, Performance of basic mixed oxides for aqueous-phase 5-hydroxymethylfurfural-acetone aldol condensation, Appl. Catal. B: Environ. 201 (2017) 221–231, https://doi.org/10.1016/j.apcatb.2016.08.013.
[18] I. Sádaba, M. Ojeda, R. Mariscal, R. Richards, M.L. Granados, Mg–Zr mixed oxides for aqueous aldol condensation of furfural with acetone: Effect of preparation method and activation temperature, Catal. Today 167 (2011) 77–83, https://doi.org/10.1016/j.cattod.2010.11.059.
[19] L. Faba, E. Díaz, S. Ordóñez, Aqueous-phase furfural-acetone aldol condensation over basic mixed oxides, Appl. Catal. B: Environ. 113–114 (2012) 201–211, https://doi.org/10.1016/j.apcatb.2011.11.039.
[20] J.D. Lewis, S. van de Vyver, Y. Román-Leshkov, Acid-base pairs in lewis acidic zeolites promote direct aldol reactions by soft enolization, Angew. Chem. Int. Ed. Engl. 54 (2015) 9835–9838, https://doi.org/10.1002/anie.201502939.
[21] O. Kikhtyanin, Z. Tišler, R. Velvarská, D. Kubička, Reconstructed Mg-Al hydrotalcites prepared by using different rehydration and drying time: physico-chemical properties and catalytic performance in aldol condensation, Appl. Catal. A: Gen. 536 (2017) 85–96, https://doi.org/10.1016/j.apcata.2017.02.020.
[22] A. Tampieri, C. Russo, R. Marotta, M. Constantí, S. Contreras, F. Medina, Microwave-assisted condensation of bio-based hydroxymethylfurfural and acetone over recyclable hydrotalcite-related materials, Appl. Catal. B: Environ. 282 (2021), 119599, https://doi.org/10.1016/j.apcatb.2020.119599.
[23] A. Tampieri, M. Lilic, M. Constantí, F. Medina, Microwave-assisted aldol condensation of furfural and acetone over Mg–Al hydrotalcite-based catalysts, Crystals 10 (2020) 833, https://doi.org/10.3390/cryst10090833.
[24] L. Dubnová, L. Smoláková, O. Kikhtyanin, J. Kocík, D. Kubička, M. Zvolská, M. Pouzar, L. Čapek, The role of ZnO in the catalytic behaviour of Zn-Al mixed oxides in aldol condensation of furfural with acetone, Catal. Today 379 (2021) 181–191, https://doi.org/10.1016/j.cattod.2020.09.011.
[25] H. Olcay, R. Malina, A.A. Upadhye, J.I. Hileman, G.W. Huber, S.R.H. Barrett, Techno-economic and environmental evaluation of producing chemicals and drop-in aviation biofuels via aqueous phase processing, Energy Environ. Sci. 11 (2018) 2085–2101, https://doi.org/10.1039/c7ee03557h.
[26] H. Chang, E.B. Gilcher, G.W. Huber, J.A. Dumesic, Synthesis of performance-advantaged polyurethanes and polyesters from biomass-derived monomers by aldol-condensation of 5-hydroxymethyl furfural and hydrogenation, Green Chem. 23 (2021) 4355–4364, https://doi.org/10.1039/d1gc00899d.
[27] A.A. Fedotov, S.A. Ugryumov, Chemical processes of structuring of furfural acetone monomer FA, Polym. Sci. Ser. D 7 (2014) 65–68, https://doi.org/10.1134/S1995421214010043.

[28] A.A. Patel, S.R. Patel, Synthesis and characterization of furfural-acetone polymers, Eur. Polym. J. 19 (1983) 231–234, https://doi.org/10.1016/0014-3057(83)90132-5.
[29] W.Y. Hernández, J. Lauwaert, P. van der Voort, A. Verberckmoes, Recent advances on the utilization of layered double hydroxides (LDHs) and related heterogeneous catalysts in a lignocellulosic-feedstock biorefinery scheme, Green Chem. 19 (2017) 5269–5302, https://doi.org/10.1039/c7gc02795h.
[30] O. Kikhtyanin, V. Kelbichová, D. Vitvarová, M. Kubů, D. Kubička, Aldol condensation of furfural and acetone on zeolites, Catal. Today 227 (2014) 154–162, https://doi.org/10.1016/j.cattod.2013.10.059.
[31] G.M. Lari, A.B.L. de Moura, L. Weimann, S. Mitchell, C. Mondelli, J. Pérez-Ramírez, Design of a technical Mg–Al mixed oxide catalyst for the continuous manufacture of glycerol carbonate, J. Mater. Chem. A 5 (2017) 16200–16211, https://doi.org/10.1039/c7ta02061a.
[32] S. Abelló, D. Vijaya-Shankar, J. Pérez-Ramírez, Stability, reutilization, and scalability of activated hydrotalcites in aldol condensation, Appl. Catal. A: Gen. 342 (2008) 119–125, https://doi.org/10.1016/j.apcata.2008.03.010.
[33] S. Abelló, F. Medina, D. Tichit, J. Pérez-Ramírez, X. Rodríguez, J.E. Sueiras, P. Salagre, Y. Cesteros, Study of alkaline-doping agents on the performance of reconstructed Mg–Al hydrotalcites in aldol condensations, Appl. Catal. A: Gen. 281 (2005) 191–198, https://doi.org/10.1016/j.apcata.2004.11.037.
[34] The discoloration of furfural, Sugar Series 13 (2000) 28-33.
[35] O. Kikhtyanin, V. Korolova, A. Spencer, L. Dubnová, B. Shumeiko, D. Kubička, On the influence of acidic admixtures in furfural on the performance of MgAl mixed oxide catalysts in aldol condensation of furfural and acetone, Catal. Today 367 (2021) 248–257, https://doi.org/10.1016/j.cattod.2020.04.022.
[36] K.I. Galkin, E.A. Krivodaeva, L.V. Romashov, S.S. Zalesskiy, V.V. Kachala, J. V. Burykina, V.P. Ananikov, Critical influence of 5-hydroxymethylfurfural aging and decomposition on the utility of biomass conversion in organic synthesis, Angew. Chem. Int. Ed. Engl. 55 (2016) 8338–8342, https://doi.org/10.1002/anie.201602883.
[37] I.Di Cosimo, Aldol reaction - heterogeneous, in: I. Horváth (Ed.), Encyclopedia of Catalysis, John Wiley & Sons, Inc, Hoboken, NJ, USA, 2002, p. 295.
[38] J. Clayden, N. Greeves, S.G. Warren. Organic Chemistry, 2nd ed., Oxford University Press, Oxford, 2012.
[39] Z. Dobi, T. Holczbauer, T. Soós, Strain-driven direct cross-aldol and -ketol reactions of four-membered heterocyclic ketones, Org. Lett. 17 (2015) 2634–2637, https://doi.org/10.1021/acs.orglett.5b01002.
[40] J.T. Kloprogge, L. Hickey, R.L. Frost, FT-Raman and FT-IR spectroscopic study of synthetic Mg/Zn/Al-hydrotalcites, J. Raman Spectrosc. 35 (2004) 967–974, https://doi.org/10.1002/jrs.1244.
[41] L. Negahdar, C.M.A. Parlett, M.A. Isaacs, A.M. Beale, K. Wilson, A.F. Lee, Shining light on the solid–liquid interface: in situ / operando monitoring of surface catalysis, Catal. Sci. Technol. 10 (2020) 5362–5385, https://doi.org/10.1039/d0cy00555j.
[42] A. Chakrabarti, M.E. Ford, D. Gregory, R. Hu, C.J. Keturakis, S. Lwin, Y. Tang, Z. Yang, M. Zhu, M.A. Bañares, I.E. Wachs, A decade+ of operando spectroscopy studies, Catal. Today 283 (2017) 27–53, https://doi.org/10.1016/j.cattod.2016.12.012.
[43] J. Horáček, Z. Tišler, U. Akhmetzyanova, P.G. Chirila, H. de Paz Carmona, The long-term performance of reconstructed MgAl hydrotalcite in the aldol condensation of furfural and acetone, React. Kinet. Mech. Catal. 133 (2021) 341–353, https://doi.org/10.1007/s11144-021-01976-z.
[44] O. Kikhtyanin, E. Lesnik, D. Kubička, The occurrence of Cannizzaro reaction over Mg-Al hydrotalcites, Appl. Catal. A: Gen. 525 (2016) 215–225, https://doi.org/10.1016/j.apcata.2016.08.007.
[45] S. Subbiah, S.P. Simeonov, J.M.S.S. Esperança, L.P.N. Rebelo, C.A.M. Afonso, Direct transformation of 5-hydroxymethylfurfural to the building blocks 2,5-dihydroxymethylfurfural (DHMF) and 5-hydroxymethyl furanoic acid (HMFA) via Cannizzaro reaction, Green Chem. 15 (2013) 2849, https://doi.org/10.1039/c3gc40930a.
[46] H. Olcay, A.V. Subrahmanyam, R. Xing, J. Lajoie, J.A. Dumesic, G.W. Huber, Production of renewable petroleum refinery diesel and jet fuel feedstocks from hemicellulose sugar streams, Energy Environ. Sci. 6 (2013) 205–216, https://doi.org/10.1039/c2ee23316a.
[47] V. Korolova, F. Ruiz-Zepeda, M. Lhotka, M. Veselý, O. Kikhtyanin, D. Kubička, Fading memory of MgAl hydrotalcites at mild rehydration conditions deteriorates their performance in aldol condensation, Appl. Catal. A: Gen. 15 (2022), 118482, https://doi.org/10.1016/j.apcata.2022.118482.
[48] A. Tampieri, M. Szabó, F. Medina, H. Gulyás, A brief introduction to the basics of NMR spectroscopy and selected examples of its applications to materials characterization, Phys. Sci. Rev. 6 (2021), https://doi.org/10.1515/psr-2019-0086.
[49] I.M. Hoodless, Isotope effect studies of the decomposition of 2-propanol on hafnium(IV) oxide, Can. J. Chem. 55 (1977) 153–157, https://doi.org/10.1139/v77-026.
[50] O. He, Y. Zhang, P. Wang, L. Liu, Q. Wang, N. Yang, W. Li, P. Champagne, H. Yu, Experimental and kinetic study on the production of furfural and HMF from glucose, Catalysts 11 (2021) 11, https://doi.org/10.3390/catal11010011.